RSC Advances

ROYAL SOCIETY OF CHEMISTRY

www.rsc.org/advances

Graphical Abstract

Anti-friction film with friction-reduction and anti-wear properties is formed under elastic deformation at the von mises stress of 917MPa (at 12 N).

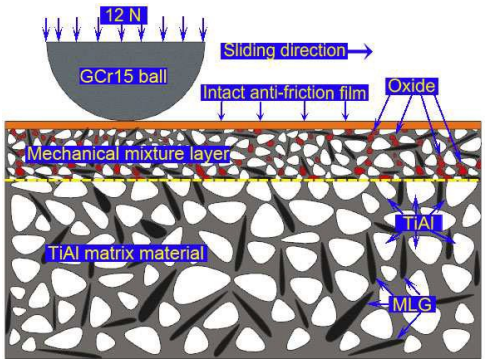

Tribological behavior of TiAl matrix self-lubricating composites reinforced by multilayer graphene

Kang Yang, Xiaoliang Shi*, Wenzheng Zhai, Long Chen, Ao Zhang, Qiaoxin Zhang

School of Mechanical and Electronic Engineering, Wuhan University of Technology, 122 Luoshi Road, Wuhan 430070, China

Abstract: Tribological performance of multilayer graphene-reinforced TiAl matrix self-lubricating composites (GTMSC) is significantly influenced by elastic and plastic deformation during the sliding wear. The primary purpose of this study is to investigate the dry tribological behaviors of GTMSC at the different applied loads. The sliding tribology tests are carried out at 4, 8, 12 and 16 N, respectively. The friction coefficients and wear rates are analyzed under the condition of elastic or plastic deformation. The elastic or plastic deformation is determined by comparing the yield stress with the von mises stress obtained by numerical simulation method. The results show that GTMSC exhibits the different tribological behaviors under the condition of elastic or plastic deformation. It is found that GTMSC shows the excellent tribological performances at 12 N for the elastic deformation resulting in the formation of anti-friction films. Nevertheless, GTMSC exhibits the poor tribological behaviors at 16 N due to the plastic deformation leading to the destruction of anti-friction films and the formation of cracks.

Keywords: Metal matrix composites, microstructure, wear resistance, friction coefficient, wear mechanism

* Corresponding author. Tel./Fax: +86-27-87651793. E-mail address: sxl@whut.edu.cn (X.L. Shi)

1. Introduction

TiAl alloys own the low density, high mechanical strength and elasticity modulus, as well as the strength retention at elevated temperature[1, 2]. Hence, TiAl alloys could be taken as the excellent structure materials of aerospace and automobile industries. For instance, aerospace components like turbine blades and automobile components like exhaust valves work at the temperature of 700 °C[3-5]. O.B. Lopez et al.[6] consider that the lower wear rate is beneficial to the improvement of the useful lifetime of materials. A. Rastkar et al.[7] study the tribological behaviors of TiAl alloys, and detect that TiAl alloys possess the high wear rates during the sliding wear. To improve the useful lifetime and enlarge the application range of TiAl alloys, it is necessary to further investigate the tribological behaviors by adding solid lubricants.

From the tribological point of view, the tribological properties of TiAl matrix self-lubricating composites (TMC) are mainly evaluated by the friction coefficients and wear rates. X.L. Shi et al.[8] investigate the tribological behaviors of TMC containing 5wt.% silver at room temperature, and find that the mean friction coefficient and wear rate are approximately 0.28 and 2.7×10^{-4} $mm^3N^{-1}m^{-1}$ at 10 N respectively. Z.S. Xu et al.[9] report the tribological properties of TMC containing 3.5wt.% multilayer graphene (MLG) at room temperature, and detect that the mean friction coefficient and wear rate are 0.32 and 0.73×10^{-4} $mm^3N^{-1}m^{-1}$ at 10 N. Comparing with TiAl alloys, the friction coefficient and wear rate of TMC containing 3.5wt.% MLG are significantly reduced by almost 4 and 7 times of magnitude. The tribological properties are more excellent for 3.5wt.% MLG, if compared to TMC

containing 5wt.% silver. Simultaneously, it is demonstrated that the tribological properties of composite materials are significantly improved by adding the MLG[10, 11]. Moreover, D. Berman et al.[12] report the tribological behaviors of 440C steel containing graphene, and find that the low friction coefficient and wear rate are obtained in the initial sliding stage at the low applied loads. L.Y. Lin et al.[13] study the frictional forces of multilayer graphene using atomic force microscopy, and detect that the frictional forces of graphene films increase from 0.36 to 0.62 nanometer Newton (nN) at the applied loads of 3-30 nN. H. Lee et al.[14] report the wear mechanism of graphene, and find that when the frictional forces exceed interlaminar binding force, the interlaminar structure of graphene is laminately destroyed during the sliding process. Simultaneously, the friction and wear properties are continually improved with the increase of graphene layers. To the best of our knowledge, the effect of applied loads on the tribological properties of TMC containing MLG is rarely reported by investigating the elastic or plastic deformation of TMC. Hence, the tribological properties of multilayer graphene-reinforced TiAl matrix self-lubricating composites (GTMSC) will be discussed under the condition of the elastic or plastic deformation of TMC.

The numerical simulation, which is an effective method to study the von mises stress of materials, is proposed to apply in the tribological field by constructing the finite element models[15, 16]. J. M. Jungk et al.[17] report the transition between elastic and plastic deformation of metallic substrate with the increase of applied loads using the numerical simulation method. J.P. Song et al.[18] construct a finite element model in

order to predict the thickness of a self-lubricating layer during the dry sliding. Hence, the finite element method could be adopted to investigate tribological properties of materials at the different von mises stress[19-21].

In this study, the disk GTMSC rotate against the GCr15 balls of 6 mm diameter at a sliding speed of 0.234 m/s. The analysis system (ANSYS) of finite element analysis software is adopted in order to obtain the von mises stresses at the applied loads of 4, 8, 12 and 16 N, respectively. The elastic or plastic deformation of GTMSC is determined by making a comparison between the von mises stress and yield stress. The tribological properties are detailedly discussed under the condition of the elastic or plastic deformation of GTMSC.

2. Experimental details

2.1 Material preparation

TiAl matrix composites (48at.% Ti-47at.% Al-2at.% Cr-2at.% Nb-1at.% B) containing 1.5wt.% MLG fabricated by spark plasma sintering (SPS) are composed of commercially available Ti (20 μm in average size, 99.9% in purity), Al (20 μm in average size, 99.9% in purity), B (25 μm in average size, 99.9% in purity), Nb (10 μm in average size, 99.9% in purity), Cr (10 μm in average size, 99.9% in purity) and MLG (thickness 40 nm in average size, lateral dimension 50 μm in average size). TiAl alloys are mainly composed of Ti and Al powders. The powders of Cr and Nb elements are added into TiAl matrix material in order to improve the high-temperature strength by the method of interstitial solution strengthening. The crack propagation could be effectively prevented by the precipitation strengthening of B element.

Powders of MLG are chosen to improve the friction-reduction and anti-wear properties of TiAl alloys, which are provided by Nanjing XFNANO material Tech Co., Ltd. Before SPS process, the vibration milling of a vibration frequency (45 Hz) is employed to mix the starting powers in the teflon vials. In pure Ar atmosphere protection, the mixtures are sintered in the cylindrical graphite mold of 20 inner diameter for 5 min by a D.R.Sinters SPS 3.20 (Sumitomo Coal & Mining, now SPS Syntex Inc.) apparatus at the temperature and pressure of 1000 ℃ and 30 MPa. Before the tribological tests, the as-sintered specimens are ground to remove the layer on the surface and polished mechanically with emery papers down to 1200 grit, and then with 0.05 μm wet polishing diamond pastes.

2.2 Vicker's microhardness and density

According to the ASTM standard E92-82[22], the hardness of as-sintered specimen is measured by a HVS-1000 Vicker's hardness instrument for a dwell time of 8 s at a load of 1 Kg. Seven tests are repeatedly carried out to obtain the mean hardness of 5.1 GPa. The mean density (3.83 g/cm^3) of as-sintered specimens is determined by Archimedes' method according to the ASTM Standard B962-08[23].

2.3 Tribological test

The tribological tests are executed on a HT-1000 ball-on-disk high temperature tribometer (made in Zhong Ke Kai Hua Corporation, China) according to the ASTM Standard G99-95[24]. After being cleaned and dried, the disks of as-sintered GTMSC rotate against the GCr15 balls of 6 mm diameter and 6.9 GPa hardness at a sliding speed of 0.234 m/s. At room temperature, the tribological tests are conducted along

the frictional orbit of 4 mm diameter for 80 min at the applied loads of 4, 8, 12 and 16 N, respectively. During the sliding wear, the friction coefficients are continually measured and recorded with the increase of real time by computer-controlled system. The wear rates can be calculated as shown in formula (1):

$$W = V/(P \cdot S) \quad (1)$$

where V is wear volume in mm^3, P is applied load in N, S is total sliding distance in mm. The wear volume V ($V=A \cdot L$) of as-sintered specimen is attained by measuring the cross-section area A and calculating the perimeter L of wear scar. When the stylus is moving across wear scar, the stylus coordinate positions are continuously recorded to form a 2D profile. The cross-section area A is acquired by calculating the area of formed 2D profile. Three tests are repeatedly executed to obtain the mean cross-section area A of one wear scar.

2.4 Analysis

The as-prepared specimen is examined to identify different phase constitutions by X-ray diffraction (XRD) with CuKα radiation at 30 KV and 40 mA at a scanning speed of $0.01°s^{-1}$. The morphologies and compositions of wear scars are analyzed by electron probe microanalysis (EPMA, JAX-8230) and energy dispersive spectroscopy (EDS, GENESIS 7000).

2.5 The finite element method and model

Fig.1(a) shows the schematic diagram of a ball-on-disk pair. The disk rotates continuously against the GCr15 balls of stationary fixation at the applied loads of 4, 8, 12 or 16 N, respectively. It could be considered that the point contact exists between

the ball and disk during the sliding wear. The contact radius is calculated by Hertzian contact equations[16]. Because the contact radius is much smaller, if compared to the circumference of wear scar, the rotational motion of disk could be treated as a periodic motion along a straight line[25]. Additionally, the finite element model, for the symmetry properties of cylindrical disk of 20 mm diameter, could be simplified into a 2D model, as shown in **Fig**.1(b). Simultaneously, the GCr15 ball is regarded as a rigid body during the numerical simulation process. The simplified disk is taken as a linear isotropic model for the heterogeneous organization structure of GTMSC.

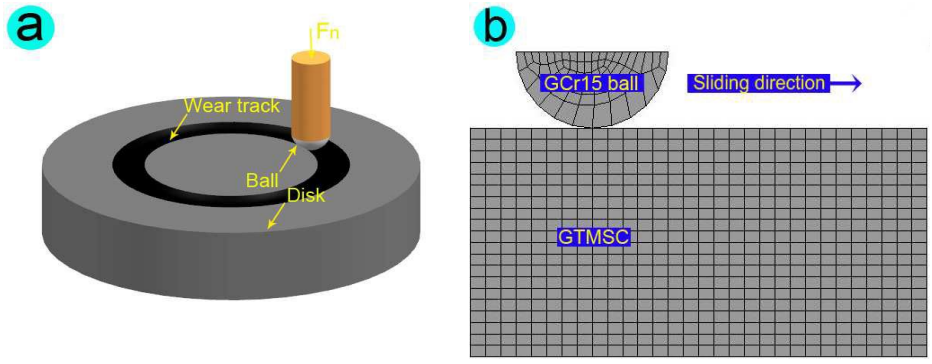

Fig.1 Schematic diagram of a ball-on-disk pair (a) and simplified 2D model (b)

3. Results and discussion

3.1 Microstructure and tribological performance of GTMSC

Fig.2(a) shows the typical FESEM image of MLG in the cross-section of GTMSC/MLG. As can be seen from in **Fig**.2(a), the MLG is tightly embedded into the bulk TiAl alloys, resulting in the improvement of mechanical properties like the higher fracture toughness and tribological performances like the lower friction coefficient and wear rate[9]. The multilayer morphologies of graphene are demonstrated by observing the multilayer structure of graphene in the area marked by rectangle in

Fig.2(a). As shown in **Fig**.2(b), the molecular structure of MLG is shown in the form of three-dimensional crystal. As is clear in XRD pattern of GTMSC in **Fig**.2(c), the as-fabricated GTMSC are mainly consisted of TiAl, C (MLG) and TiC according to the different intensity of diffraction peaks of respective phases.

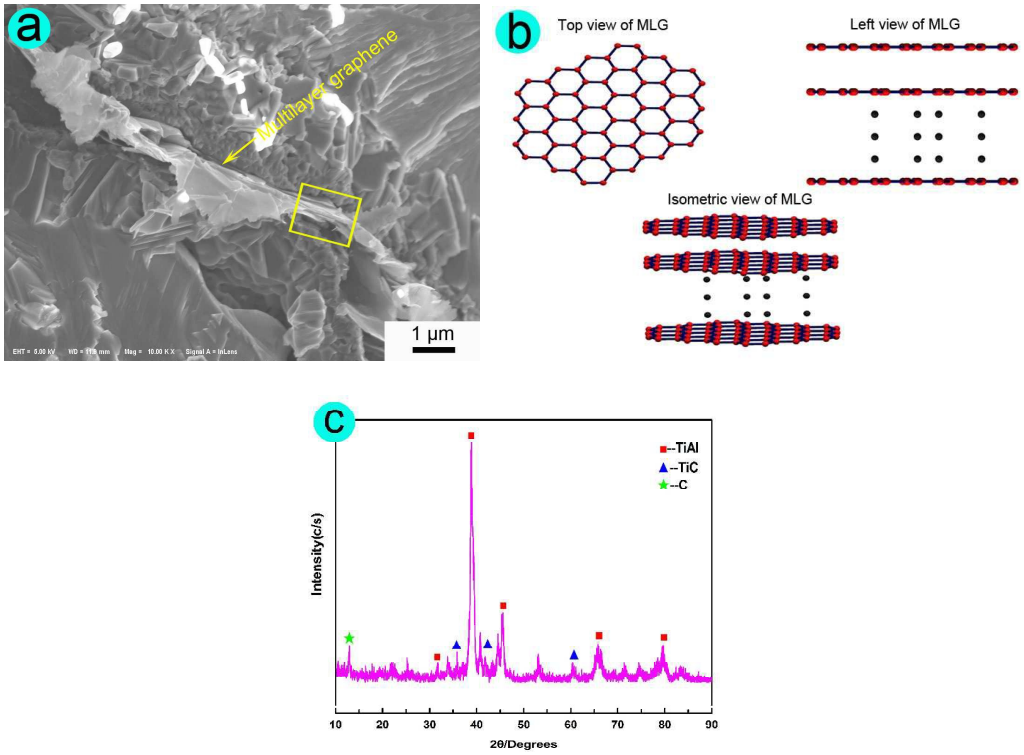

Fig.2 (a) Typical FESEM image of MLG in the cross-section of GTMSC/MLG; (b) Molecular structure of MLG; (c) XRD pattern of GTMSC fabricated by SPS

Fig.3 shows the microstructure and elemental distributions of GTMSC. As shown in **Fig**.3(c), it could be seen from the distribution of C element that MLG is uniformly distributed in GTMSC.

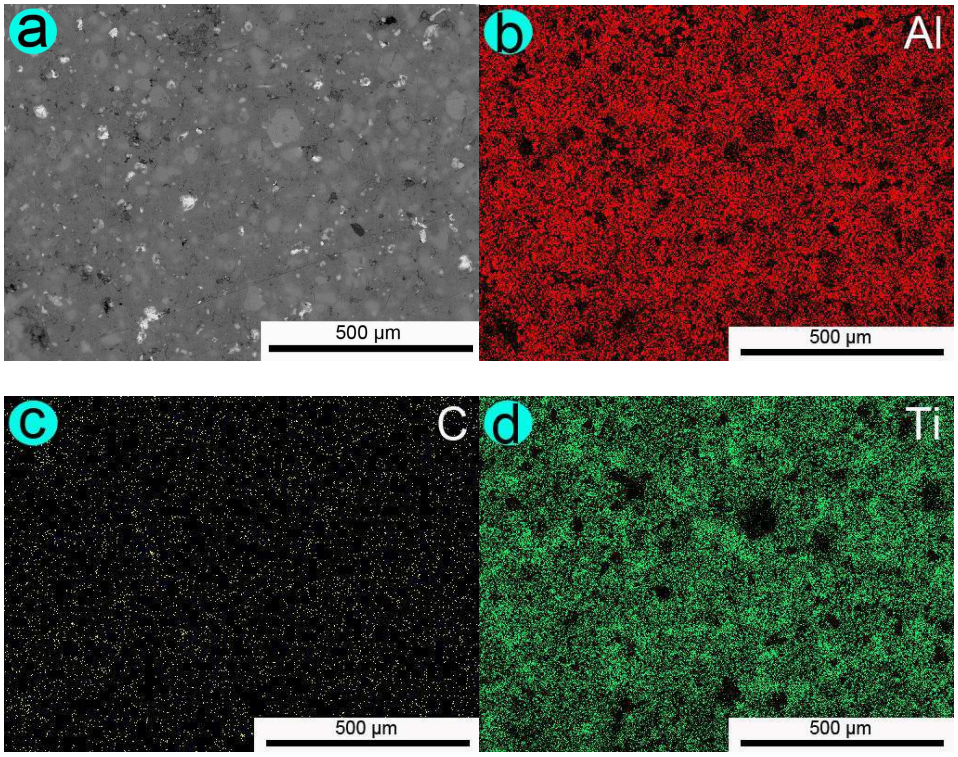

Fig.3 Microstructure and elemental distributions of GTMSC

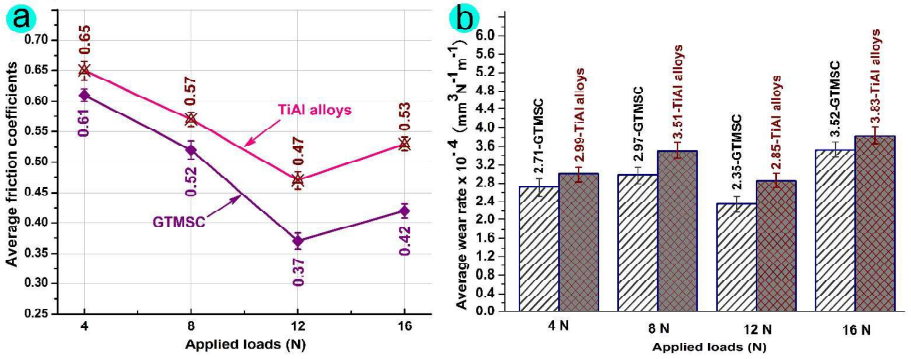

Fig.4 Variation of friction coefficients and wear rates of GTMSC/TiAl alloys after 80 min tests at the different applied loads: friction coefficients (a) and wear rates (b)

Fig.4 shows the variation of friction coefficients and wear rates of GTMSC/TiAl alloys after 80 min tests at the different applied loads. As can be clearly seen from **Fig**.4, the tribological performances of GTMSC are dramatically improved by the excellent mechanical properties and tribological performances of MLG, if compared

to those of TiAl alloys. During the sliding wear, the multilayer structure of graphene is separated layer by layer, and then spread out on the wear scar to hinder the direct contact of GCr15 balls and GTMSC disks, resulting in the lower friction coefficient and wear rate. During the sliding process, the MLG with the high hardness could protect from the destruction of GTMSC to further improve the tribological properties by dissipating the stress and preventing the crack propagation[9]. Hence, the fracture toughness of GTMSC is reinforced by the laminar structure MLG. The tribological properties of GTMSC are respectively obtained at the applied loads of 4, 8, 12 and 16 N as follows.

- 4 N: The mean friction coefficient and wear rate are 0.61 and 2.71×10^{-4} $mm^3N^{-1}m^{-1}$ respectively.
- 8 N: The friction coefficient reduces down to 0.52, while the wear rate increases up to 2.97×10^{-4} $mm^3N^{-1}m^{-1}$ with the increase of applied loads from 4 to 8 N.
- 12 N: The lower friction coefficient (0.37) and smaller wear rate (2.35×10^{-4} $mm^3N^{-1}m^{-1}$) are attained at the applied loads of 12 N.
- 16 N: The friction coefficients (0.42) and wear rates (3.52×10^{-4} $mm^3N^{-1}m^{-1}$) significantly increase at 16 N, if compared to the friction coefficient of 0.37 and wear rate of 2.35×10^{-4} $mm^3N^{-1}m^{-1}$ at 12 N.

3.2 The FEM results

Many parameters of GTMSC are needed to choose for the numerical simulation in advance. The three tests are carried out to obtain the mean elasticity modulus of 96 GPa using the nanomechanical testing instrument of Hysitron TI-950 (made in HYSITRON

Corporation, America). The mean yield stress of 1165 MPa are obtained by executing three tests using the material testing machine of INSTRON1341 (made in Instron Corporation, Britain). The elasticity modulus of the GCr15 ball is 200 GPa. The poisson's ratios of GCr15 ball and GTMSC are 0.30 and 0.36 respectively. Furthermore, PLANE183 could be chosen as the element type of disk for its properties of plasticity, large deflection and large capabilities. In this study, the element type of TARGE169 and CONTA172 are chosen for surface-surface contact of GTMSC and GCr15 ball.

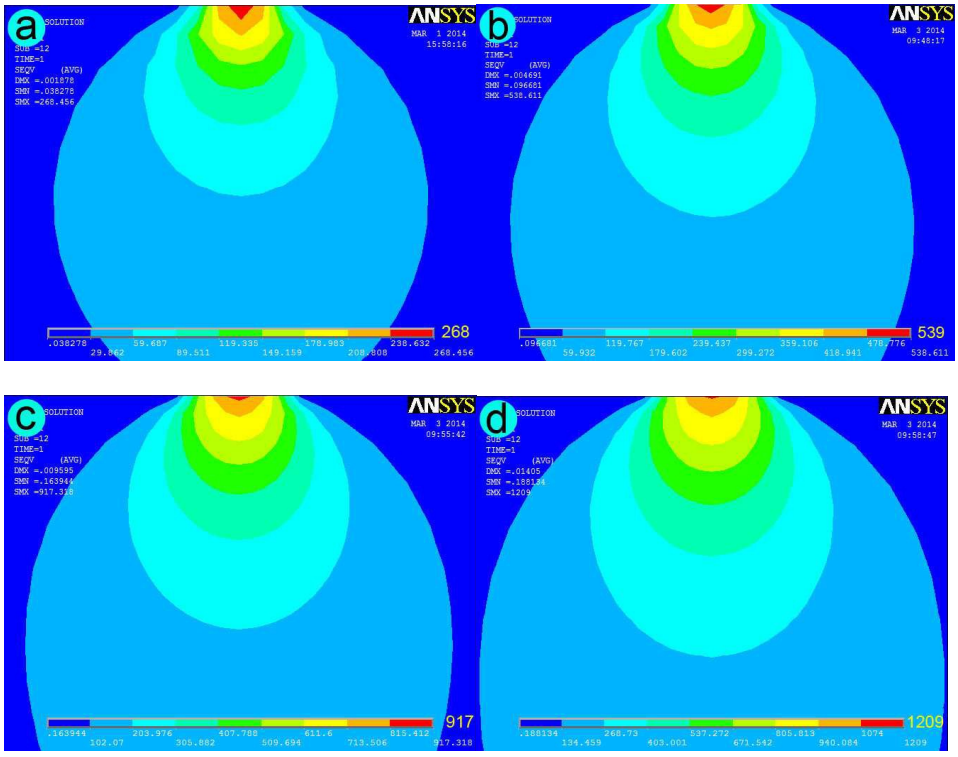

Fig.5 Von mises stresses of GTMSC at different applied loads: 4 N (a), 8 N (b), 12 N (c) and 16 N (d)

Fig.5 shows the von mises stresses of GTMSC at different applied loads. As shown in **Fig**.5, it could be obviously seen that the von mises stress is significantly

increscent and its influenced zones are continuously enlarged with the increasing of applied loads from 4 to 16 N. The GTMSC has the low von mises stress (268 MPa) at 4 N. When the applied load increases up to 8 N, the von mises stress is 539 MPa. The applied load of 12 N is chosen to obtain the von mises stress of 917 MPa. The von mises stress (1209 MPa) of GTMSC is higher than yield stress (1165 MPa) at the applied load of 16 N. Basing on above discussion, the elastic deformation of GTMSC appears at applied loads of 4, 8 and 12 N, while the plastic deformation happens at 16 N.

3.3 Wear mechanism of GTMSC

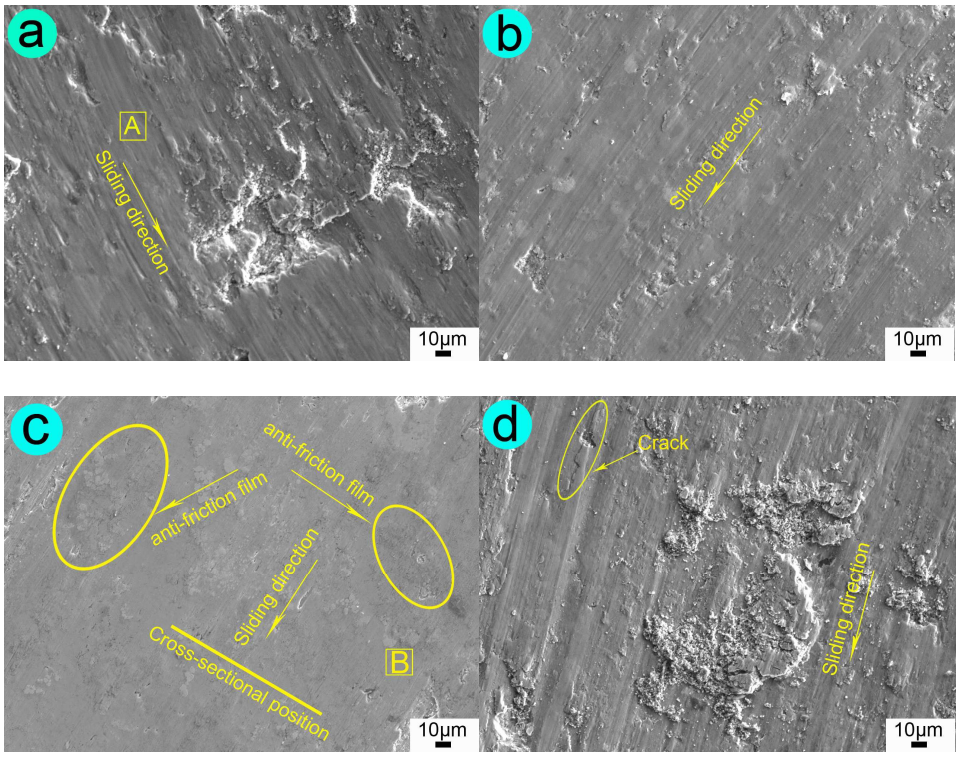

Fig.6 Typical EPMA morphologies of wear scars of GTMSC after 80 min tests at the different applied loads of 4 (a), 8 (b), 12 (c) and 16 N (d)

Table 1 EDS analysis of elements (wt.%) in the areas marked by rectangles in **Fig**.6

area	Ti	Al	Cr	Nb	B	C	O
A (4 N)	53.6	30.4	2.2	4.2	0.5	2.2	6.9
B (12 N)	49.5	30.5	2.1	4.3	0.4	5.3	7.9

Fig.6 exhibits the typical EPMA morphologies of wear scars of GTMSC after 80 min tests at the applied loads of 4, 8, 12 and 16 N. Because the low von mises stress (268 MPa) is not able to repair the grooves and pits during the sliding process, some parallel grooves, obvious pits and a few wear debris exist on worn surface, as shown in **Fig**.6(a). It is obvious that the main wear mechanisms are furrow and peeling. **Table** 1 shows the EDS analysis of elements (wt.%) in the areas marked by rectangles in **Fig**.6. Elementary composition of Ti53.6-Al30.4-Cr2.2-Nb4.2-B0.5-C2.2-O6.9 (in wt.%) appears in the marked area A in **Fig**.6(a). The appearance of oxygen element (O) shows that oxidation reaction has happened during the sliding process. F.H. Stott et al.[26] believe that the formation of oxidation layers is beneficial to the reduction of wear rates. As can be seen in **Fig**.4, at the applied load of 4 N, the mean friction coefficient and wear rate of GTMSC are approximately 0.61 and 2.71×10^{-4} $mm^3N^{-1}m^{-1}$ respectively. Hence, it could be reasonably concluded that the generated oxidized particles lower wear rate, while is not related with friction coefficient.

As shown in **Fig**.6(b), at the applied load of 8 N, the worn surface becomes much smoother, and the grooves become fine and shallow. Y.J. Yu et al.[27] study the tribological behaviors of NiAl intermetallic compound coatings, and detect that the worn surface becomes much smoother with the increase of applied loads. The main wear mechanisms should be furrow and delamination at 8 N. Hence, it may be

concluded from the EPMA morphology of wear scar that the morphology of wear scar is improved at the von mises stress of 528 MPa (at 8 N), while the smooth wear scar is not obtained for the poor reparation abilities.

As shown in **Fig**.6(c), with the increasing of applied loads from 8 to 12 N, a few shallow peeling pits and anti-friction films (tribo-films) appear on the smooth worn surface. It is apparent that the primary wear mechanism is slight peeling. As shown in **Table** 1, the existence of oxygen and carbon element (O and C) of the marked area B in **Fig**.6(c) demonstrates that the anti-friction films contain massive oxides and MLG with the lubricating property. It may be concluded that the von mises stress of 917 MPa (at 12 N) could refine wear debris, repair wear scar and be beneficial to the formation of tribo-films. S.Y. Zhu et al.[28] report that the smooth tribo-film is beneficial to friction-reduction and anti-wear properties. Hence, the lower friction coefficient (0.37) and wear rate (2.35×10^{-4} $mm^3N^{-1}m^{-1}$) are obtained at 12 N for the existence of tribo-films.

When the applied load increases up to 16 N, as shown in **Fig**.6(d), the deep grooves, obvious cracks, abundant wear debris and severe delamination appear on the rough wear scar. It is obvious that the main wear mechanisms are fracture and plough. The high von mises stress (1209 MPa) obtained at 16 N exceeds the yield stress (1165 MPa) of GTMSC. Consequently, it could be believed that the plastic deformation results in the high wear rate (3.52×10^{-4} $mm^3N^{-1}m^{-1}$) and obvious cracks of GTMSC. F. Akhtar et al.[29] investigate the microstructure evolution and wear properties of steel matrix composites reinforced by TiB_2 and TiC, and detect that the cracks and weight

loss significantly increase for the plastic deformation of steel matrix composites. A.R. Rastkar et al.[7] study the sliding wear behaviors of TiAl alloys, and find that a great many fine debris appear on wear scar for the interlamellar cracks and plastic deformation. Hence, it could be reasonably concluded that the formation of the cracks are caused by the plastic deformation of GTMSC. During the dry wear, the cracks gradually peel off from GTMSC and spread out to worn surface at the applied load of 16 N, and then the big crack debris is crushed into massive wear particles at the high pressures of asperity contact zone. Although the action of third body of wear debris is beneficial to the reduction of friction coefficients and wear rates, the friction coefficients (0.42) and wear rates (3.52×10^{-4} $mm^3N^{-1}m^{-1}$) significantly increase for the destruction of tribo-film at 16 N, if compared to the friction coefficient (0.37) and wear rate (2.35×10^{-4} $mm^3N^{-1}m^{-1}$) at 12 N.

Basing on aforementioned discussions about the friction coefficient, wear rate, von mises stress and wear scar of GTMSC, some results can be obtained. (1) The von mises stresses continually increase with the increasing of applied loads from 4 to 16 N. (2) A fewer wear debris appear on the smoother wear scar with an increase in applied loads ranged from 4 to 12 N, while the massive wear debris exist on the rough worn surface at 16 N for the cracks and plastic deformation of GTMSC. (3) The wear rates are smaller under the condition of elastic deformation of GTMSC, if compared to the plastic deformation. The friction coefficients constantly reduce with the increase of applied loads of 4-12 N, and then slightly increase at 12-16 N. (4) Excellent tribological properties are obtained for the formation of anti-friction films at 12 N.

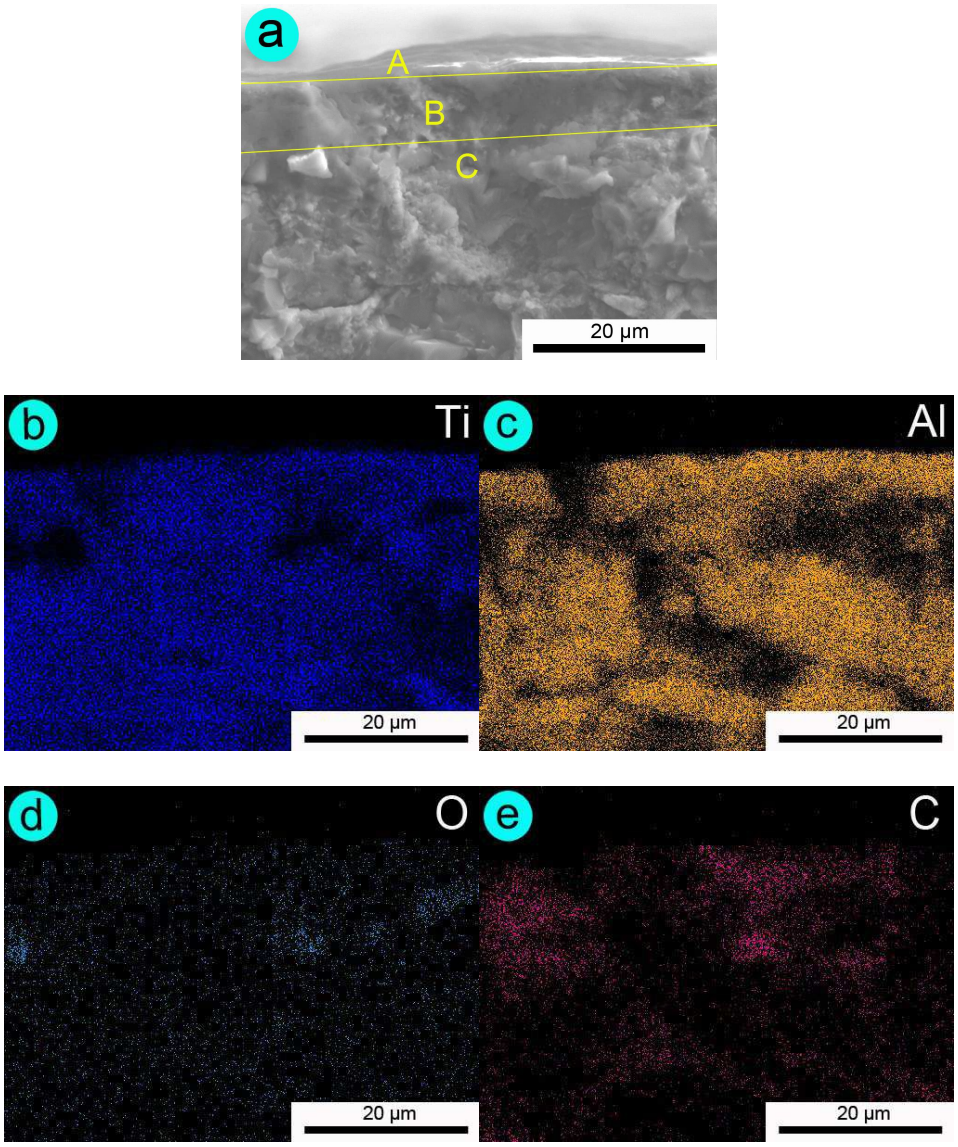

Fig.7 EPMA micrograph and elemental distribution of cross-section of wear scar of GTMSC after 80 min tests at 12 N

To further investigate the formation of anti-friction films at 12 N, as shown in **Fig**.7, the typical EPMA micrograph and elemental distribution of cross-section of wear scar of GTMSC after 80 min tests at 12 N are observed. The position of cross-section of wear scar at 12 N is marked by straight line (see **Fig**.6(c)). The significant stratification morphologies are marked as three layers of A, B and C, as

shown in **Fig**.7(a). It could be found that layer A, for the primary wear mechanisms of slight peeling, is an intact anti-friction film. Layer B shows the thin compacted layer consisting of submicron grains. While layer C is composed of large grains. **Fig**.7(b-e) show the elemental distributions of cross-section of wear scar. As is clear in **Fig**.7(e), the C element is mainly distributed in the zones marked by A and B in **Fig**.7(a). Consequently, it could be believed that the tribological properties of GTMSC at 12 N are significantly improved by the anti-friction film and thin compacted layer containing massive MLG. Z.S. Xu et al.[9] also detect that the formation of tribo-film composed of MLG is contribute to the decrease of friction coefficient and wear rate. D. Berman et al.[30] also consider that during the sliding process, the wear debris containing MLG are spread out on wear scar to form an anti-friction film, resulting in the lower friction coefficient and wear rate.

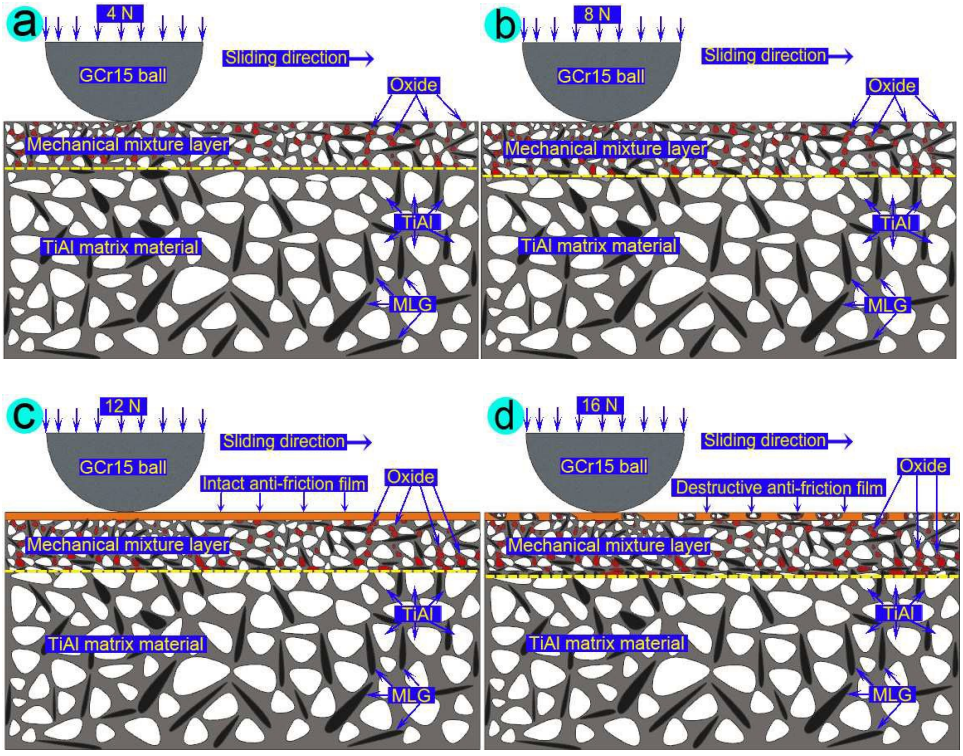

Fig.8 Schematic diagrams of the microstructures of cross-sections of wear scars at the different applied loads: 4 N (a), 8 N (b), 12 N (c) and 16 N (d)

Fig.8 shows the schematic diagrams of the microstructures of cross-sections of wear scars at the different applied loads. As can be seen from **Fig**.8(a-b), the thickness of mechanical mixture layers constantly increase with the increase of applied loads from 4 to 8 N. As shown in **Fig**.8(c), the significant stratification morphologies of the anti-friction film, mechanical mixture layer and TiAl matrix material, which are corresponding to the layers A, B and C in **Fig**.7(a), are clearly observed after 80 min sliding at 12 N. As can be seen from **Fig**.8(d) (at 16 N), the anti-friction film with the friction-reduction and anti-wear properties is dramatically destroyed for the plastic deformation and cracks of GTMSC at the von mises stress of 1209 MPa. Consequently, basing on above-mentioned discussion, it could be concluded that the formation of anti-friction film is in close relation with the von mises stresses generated at the applied loads of 4, 8, 12 and 16 N. The small von mises stresses of 268 and 528 MPa (at 4 and 8 N) are not able to form anti-friction films for the poor reparation ability, while the high stress (1209 MPa) destroy the formed anti-friction films for the plastic deformation and cracks of GTMSC at 16 N. The von mises stress of 917 MPa (at 12 N) is beneficial to the formation of anti-friction film, resulting in the lower friction coefficient and wear rate.

In this study, in order to investigate the tribological behaviors of multilayer graphene-reinforced TiAl matrix self-lubricating composites (GTMSC) at room temperature, the numerical simulations and experiments are carried out at the applied

loads of 4, 8, 12 and 16 N, respectively. The wear rates of GTMSC under the condition of the elastic deformation (4-12 N) are smaller than those under the plastic deformation (16 N). The friction coefficients continually reduce with an increasing in applied loads from 4 to 12 N, and then slightly increase at 12-16 N. The excellent tribological properties are attained for the formation of anti-friction films at 12 N. The formation of anti-friction films is closely related with the von mises stress. The small von mises stress is not able to form anti-friction films at 4-8 N, while the high stress destroy the formed anti-friction films at 16 N.

4. Conclusions

Multilayer graphene-reinforced TiAl matrix composites (GTMSC) are fabricated by SPS for 5 min at the temperature and pressure of 1000 ^{o}C and 30 MPa in pure Ar atmosphere protection. The tribological properties of GTMSC are investigated at the applied loads of 4, 8, 12 and 16 N, respectively. The following conclusions are obtained. (1) The excellent tribological properties are obtained for the formation of anti-friction films at 12 N. (2) The formation of anti-friction films is closely related with von mises stress. (3) A fewer wear debris appear on the smoother wear scar with the increasing of applied loads from 4 to 12 N, while the massive wear debris exist on the rougher worn surface for the plastic deformation and cracks of GTMSC at 16 N. (4) The wear rates of GTMSC are smaller under the condition of the elastic deformation at 12 N, if compared to the plastic deformation at 16 N. The friction coefficient constantly reduces with the increase of applied loads in the range of 4-12 N, and then slightly increases at 12-16 N.

Acknowledgments

This work was supported by the National Natural Science Foundation of China (51275370). The authors also wish to gratefully thank the Material Research and Testing Center of Wuhan University of Technology for their assistance.

References

1 X.H. Wu, Intermetallics, 2006, **14**, 1114.

2 C.M. Austin, Science, 1999, **4**, 239.

3 T. Kawabata, H. Fukai, O. Izumi, Acta Materialia, 1998, **46**, 2185.

4 J. Zollinger, J. Lapin, D. Daloz, H. Combea, Intermetallics, 2007, **15**, 1343.

5 G. Das, H. Kestler, H. Clemens, P. Bartolotta. Met. Mater. Soc, 2004, **56**, 42.

6 O.B. Lopez, A. Pajares, P.J. Constantino, B.R. Lawn, J. Mech. Behav. Biomed. Mater, 2014, **37**, 226.

7 A. Rastkar, A. Bloyce and T. Bell, Wear, 2000, **240**, 19.

8 X.L. Shi, Z.S. Xu, W. Wang, W.Z. Zhai, J. Yao, S.Y. Song, A.Q.U. Din and Q.X. Zhang, Wear, 2013, **303**, 486.

9 Z.S. Xu, X.L. Shi, W.Z. Zhai, J. Yao, S.Y. Song and Q.X. Zhang, Carbon, 2014, **67**, 168.

10 Y.T. Peng, Z.Q. Wang, RSC Adv., 2014, **4**, 9980.

11 Y. Zhang, H. Tang, X.R. Ji, C.S Li, L. Chen, D. Zhang, X.F Yang and H.T Zhang, RSC Adv., 2013, **3**, 26086.

12 D. Berman, A. Erdemir and A.V. Sumant, Carbon, 2013, **59**, 67.

13 L.Y. Lin, D.E. Kim, W.K. Kim and S.C. Jun, Surf. Coat. Technol., 2011, **205**, 4864.

14 H. Lee, N. Lee, Y. Seo, J. Eom and S.W. Lee, Nanotechnology, 2009, **20**, 325701.

15 A. Rezaei, W.V. Paepegem, P.D. Baets, W. Ost and J. Degrieck, Wear, 2012, **296**, 660.

16 V. Hegadekatte, N. Huber and O. Kraft, Sci. Eng., 2004, **13**, 57.

17 J.M. Jungk, J.R. Michael and S.V. Prasad, Acta. Mater., 2008, **56**, 1956.

18 J.P. Song, M. Valefi, M.D. Rooij and D.J. Schipper, Wear, 2010, **268**, 1072.

19 G. Straffelini, M. Pellizzari and A. Molinari, Wear, 2004, **256**, 754.

20 R. Tyagi, D.S. Xiong and J.L. Li, Wear, 2011, **270**, 423.

21 X.L. Shi, M. Wang, W.Z. Zhai, Z.W. Zhu, Z.S. Xu, Q.X. Zhang, S.Y. Song and J. Yao, Wear, 2013, **303**, 9.

22 ASTM E92-82, Standard test method for vickers hardness of metallic materials, ASTM International, 2003.

23 ASTM B962-08, Standard test methods for density of compacted or sintered powder metallurgy (PM) products using Archimedes' principle, ASTM International, 2008.

24 ASTM G99-95, Standard test method for wear testing with a pin-on-disk apparatus, ASTM International, 1995.

25 W. Yan, N.P. O'Dowd and E.P. Busso, J. Mech. Phys. Solids, 2002, **50**, 449.

26 F.H. Stott, Tribol. Int., 1998, **31**, 61.

27 Y.J. Yu, J.S. Zhou, J.M. Chen, H.D. Zhou, C. Guo, L.Q. Wang and L.B. Yang, Wear, 2012, **274**, 298.

28 S.Y. Zhu, Q.L. Bi, J. Yang and W.M. Liu, Tribol. Lett., 2011, **43**, 55.

29 F. Akhtar, J. Alloys. Compd., 2008, **459**, 491.

30 D. Berman, A. Erdemir and A.V. Sumant, Carbon, 2013, **54**, 454.